Heliyon 9 (2023) e13216

Contents lists available at ScienceDirect

Heliyon

journal homepage: www.cell.com/heliyon

Research article

Homocysteine-induced endoplasmic reticulum stress activates FGF21 and is associated with browning and atrophy of white adipose tissue in *Bhmt* knockout mice

Manya Warrier [a], Evan M. Paules [a,c], Jorge Silva-Gomez [a], Walter B. Friday [a], Frances Bramlett [a], Hyunbae Kim [b], Kezhong Zhang [b], Isis Trujillo-Gonzalez [a,c,*]

[a] Department of Nutrition, UNC Nutrition Research Institute, UNC-Chapel Hill, Kannapolis, NC, USA
[b] Center for Molecular Medicine and Genetics, Wayne State University School of Medicine, Detroit, MI, USA
[c] Department of Nutrition, Gillings School of Global Public Health, University of North Carolina at Chapel Hill, Chapel Hill, NC, 27514, USA

ARTICLE INFO

Keywords:
Betaine-homocysteine *S*-Methyltransferase
Lipodystrophy
ER stress
CREBH
BHMT
FGF21
Homocysteine

ABSTRACT

Betaine-homocysteine methyltransferase (BHMT) catalyzes the transfer of methyl groups from betaine to homocysteine (Hcy), producing methionine and dimethylglycine. In this work, we characterize *Bhmt* wild type (*Bhmt*-WT) and knockout (*Bhmt*-KO) mice that were fully backcrossed to a C57Bl6/J background. Consistent with our previous findings, *Bhmt*-KO mice had decreased body weight, fat mass, and adipose tissue weight compared to WT. Histological analyses and gene expression profiling indicate that adipose browning was activated in KO mice and contributed to the adipose atrophy observed. BHMT is not expressed in adipose tissue but is abundant in liver; thus, a signal must originate from the liver that modulates adipose tissue. We found that, in *Bhmt*-KO mice, homocysteine-induced endoplasmic reticulum (ER) stress is associated with activation of the hepatic transcription factor cyclic AMP response element binding protein (CREBH), and an increase in hepatic and plasma concentrations of fibroblast growth factor 21 (FGF21), which is known to induce adipose browning. Our data indicate that the deletion of a single gene in one-carbon metabolism modifies adipose biology and energy metabolism. Future studies could focus on identifying if functional polymorphisms in *BHMT* result in a similar adipose atrophy phenotype.

1. Introduction

Betaine-homocysteine *S*-methyltransferase (BHMT) is an important Zn-dependent thiol-methyltransferase that catalyzes the formation of methionine from homocysteine using betaine as its methyl donor [1,2]. Methionine is subsequently converted to *S*-adenosylmethionine (SAM) and is used for various methylation reactions [3]. BHMT is one of the most abundant proteins in the liver, amounting to 0.6–1% of total protein [4], and it is also found in kidney, the eye lens, and at lower activities in other tissues, but not in adipose [5,6]. Mice in which *Bhmt* was deleted (whole body; *Bhmt*-KO) have increased hepatic concentrations of the enzymatic substrates betaine and homocysteine (Hcy) [5,7]. Moreover, at 5 weeks of age, hepatic and plasma concentrations of triacylglycerol (TAG) are higher in *Bhmt*-KO compared to wild type [5]. These KO mice have better glucose uptake and insulin tolerance than wild

* Corresponding author. Department of Nutrition, UNC Nutrition Research Institute, UNC-Chapel Hill, Kannapolis, NC, USA.
E-mail address: isis_trujillo@unc.edu (I. Trujillo-Gonzalez).

https://doi.org/10.1016/j.heliyon.2023.e13216
Received 2 November 2022; Received in revised form 13 January 2023; Accepted 20 January 2023
Available online 28 January 2023

Nomenclature

Abbreviations

ATF3	Activating Transcription Factor 3
BAT	Brown adipose tissue
BHMT	Betaine Homocysteine-S-Methyltransferase
CAC	Cachexia
CHOP	c/EPB homologous protein
CIDEA	Cell death-inducing DFFA-like effector A
CREBH	Cyclic AMP response element binding protein H
ER	Endoplasmic Reticulum Stress
FGF21	Fibroblast Growth Factor 21
Hcy	Homocysteine
KLB	β-Klotho
PCG-α	Peroxisome Proliferator-activated receptor gamma coactivator 1-alpha
SAM	S-adenosylmethionine
UCP1	Uncoupling Protein 1
WAT	White adipose tissue

types at 7 weeks of age. Additionally, KO mice develop increased energy expenditure, lipodystrophy and fatty liver compared to their wild type (WT) littermates [5,7]. At 1 year of age, 64% of *Bhmt*-KO mice develop hepatic tumors [5,7].

Though the mechanisms underlying the hepatocarcinogenesis in the *Bhmt*-KO mice have been explored [3], those involved in adipose wasting have not been addressed. We do so in this paper.

The capacity of white adipose tissue (WAT) to elevate its metabolic rate, by increased expression of UCP1 mRNA, and subsequently become brown adipose tissue (BAT) [8,9], gained attention due to the potential benefits to promote weight loss. Several factors are known to induce browning, including foods, environmental stimuli, and hormones like FGF21, by interacting with FGF receptor [10–12]. Sustained energy expenditure from WAT to BAT conversion is responsible for muscle and fat atrophy [13]. This is the major

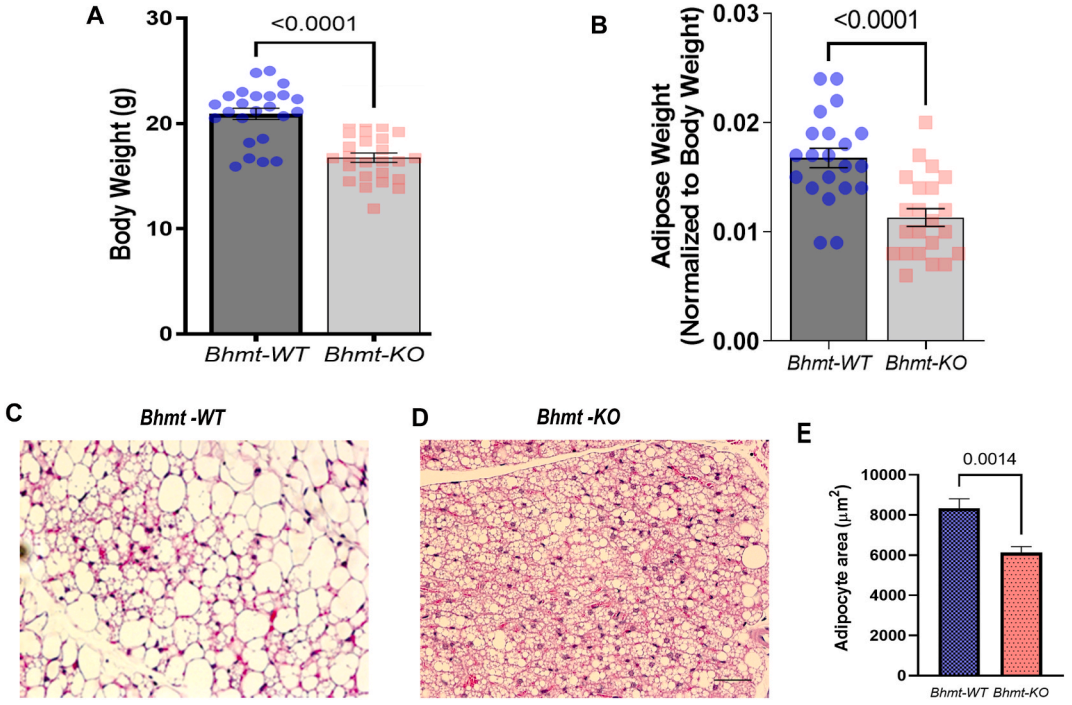

Fig. 1. Lack of the *Bhmt* gene induces adipose atrophy in mice. (A) Body weight loss of *Bhmt* knockout (*Bhmt*-KO) compared to *Bhmt* wild type (*Bhmt*-WT). (B) Adipose weight normalized over body weight. $n = 25$ *Bhmt*-KO; $n = 24$ *Bhmt*-WT. Results are presented as mean ± SEM. P values were calculated by unpaired *t*-test. (C) and (D). Representative stainings of sections from inguinal white adipose tissue (iWAT) from *Bhmt*-WT (C) and *Bhmt*-KO (D) Scale bar = 50 µm. (E) Adipocyte area quantification of iWAT from *Bhmt*-WT vs *Bhmt*-KO. Results are presented as mean ± SEM. n = 3 *Bhmt*-KO and n = 3 *Bhmt*-WT, at least 50 cells were quantified per mouse. P value was calculated by Kolmogorov-Smirnov test.

cause of cancer associated cachexia (CAC), a major cause of lean body in cancer patients that cannot be reversed by nutritional approaches, where energy wasting and hypermetabolism is observed [8,14]. In this study, we show that deletion of *Bhmt* in mice results in increased Hcy concentrations in tissues, and this is associated with the initiation of a signaling cascade involving endoplasmic reticulum stress (ER stress) and leading to expression of genes including fibroblast growth factor 21 (*Fgf21*). Previously, we reported increased Fgf21 concentrations produced by the liver in *Bhmt*-KO mice [7]. Fgf21 stimulates adipose browning and energy expenditure by upregulating the expression of the transcriptional co-activator peroxisome proliferator-activated receptor gamma coactivator -**1**-alpha (Pgc-1α), as well as uncoupling protein 1 (Ucp1). This culminates in adipose wasting in *Bhmt*-KO mice.

2. Results

2.1. Deletion of Bhmt promotes adipose atrophy in fully backcrossed mice

We previously reported that *Bhmt* knockout mice on a mixed 129/SV x C57BL/6J background (generations F3–F5), between 7 and 12 weeks of age, had reduced adipose mass and smaller-sized adipocytes [7]. Since genetic background of mice can have a profound influence on the metabolic phenotype of mice [15], we sought to re-examine this lipodystrophy phenotype after backcrossing *Bhmt*-KO mice to C57Bl/6 to generate a near congenic (99.74%) line. In this near congenic line, we confirmed that, in the *Bhmt*-KO compared to wild type (WT), there was a significant reduction in total body weight (Fig. 1A) and adipose weight (Fig. 1B) in mice (7–8 weeks of age). Histological analysis of adipose tissue taken from *Bhmt*-KO mice showed reduced adipocyte cell area in inguinal white adipose tissue (iWAT) as compared to WT (Fig. 1C–E). Adipose atrophy is characterized by reduced fat/lean mass and the 'slimming of adipocytes' in both size and volume [16], and our data show that this process is dependent on *Bhmt* status.

2.2. Adipose atrophy in Bhmt-KO mice is associated with adipose browning in inguinal adipose depots

Since smaller adipocytes and increased whole body energy expenditure and heat production are classical features of browning of WAT [17], and since adipose browning is known to promote adipose atrophy in several mouse models [8,17–20], we sought to determine if the WAT atrophy observed in *Bhmt*-KO mice is due to WAT browning. We first measured molecular markers that are frequently associated with adipose browning [21–23]. Uncoupling Protein 1 (*Ucp1)* mRNA (Fig. 2A) along with mRNA for other thermogenic genes such as Peroxisome proliferator-activated receptor gamma coactivator 1-alpha (*Pgc-1α)* and the lipid-droplet-associated protein cell death-inducing DFFA-like effector A (*Cidea*) (Fig. 2B and C) were all significantly upregulated in iWAT collected from *Bhmt*-KO mice compared to WT. Together, these results indicate that lack of *Bhmt* is sufficient to induce the expression of adipose browning markers.

2.3. Bhmt-KO livers have increased homocysteine concentrations

Plasma total Hcy concentrations were significantly increased in *Bhmt*-KO mice on a mixed 129/SV x C57BL/6J background (generations F3–F5), as we previously reported [7]. We now show that, in the fully backcrossed *Bhmt*-KO mice, both plasma Hcy concentrations (~11 fold) and liver Hcy concentrations (~2 fold) were increased in KO compared to WT mice (Fig. 3A and B). Thus, loss of *Bhmt* results in the accumulation of plasma and liver Hcy.

2.4. Bhmt-KO livers have increased ER stress and have more activated CREBH

Because high tissue Hcy is a known cause of ER stress, which in turn regulates several transcription factors residing in the ER [24,25], we investigated if *Bhmt*-KO mice have increased ER stress compared to WT. We measured gene expression of Activating

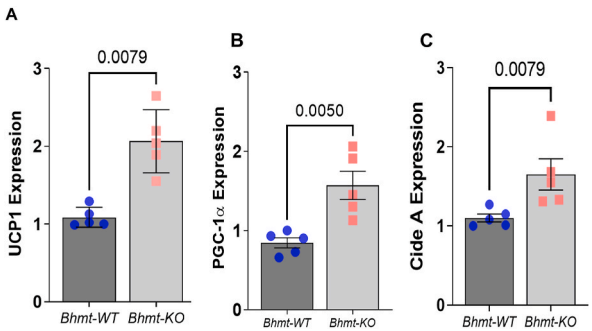

Fig. 2. Lack of the *Bhmt* gene induces the expression of beige remodeling markers that induce browning. mRNA levels of beige remodeling markers *Ucp1* (A), *Pgc1a* (B), and *Cidea* (C) in inguinal adipose tissue (iWAT) of *Bhmt*-WT and *Bhmt*-KO mice. Relative quantitative values (normalized to 36B4) are reported as fold change. Results are presented as mean ± SEM. P values were calculated by Mann-Whitney test (A and C) and by unpaired *t*-test (B). n = 5 mice per group; per genotype.

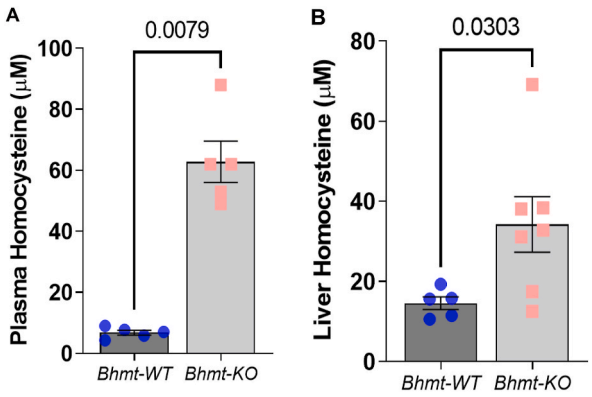

Fig. 3. Increase in plasma and liver homocysteine (Hcy) levels in *Bhmt*-KO mice. (A) Plasma levels of Hcy are increased in *Bhmt*-KO mice ~50 fold when compared with *Bhmt*-WT mice. $n = 5$ per group. (B) Liver Hcy levels were also increased ~20 fold in *Bhmt*-KO mice when compared with *Bhmt*-WT. $n = 7$ *Bhmt*-KO; $n = 5$ *Bhmt*-WT. Results are presented as mean ± SEM. P values were calculated by Mann-Whitney test.

Transcription Factor 3 (ATF3), and DNA damage-inducible transcript 3, also known as C/EBP homologous protein (CHOP), as indicators of ER stress [26–36]. We found that expression of these genes was increased 3-fold and a tendency of1.5-fold, respectively, in *Bhmt*-KO compared to WT mouse livers (Fig. 4A and B). Since changes in CHOP mRNA expression where modest, we evaluated CHOP protein levels and found an increase of ~30-fold in KO compares to WT (Fig. 4C and D; uncropped western blot Supplementary Fig. S1A). Thus, *Bhmt*-KO mice have increased ER stress compared to their WT counterparts.

Next we identified transcription factors that reside in the ER, and are produced in response to ER stress, and regulate FGF21. We found that the hepatic transcription factor known as Cyclic AMP Responsive Element Binding Protein – H (CREBH) fulfilled the above criteria [25,37,38]. We measured full length and activated CREBH in the liver lysates prepared from both *Bhmt*-WT and KO mice by Western blot analysis and found that the cleaved, activated form of CREBH was significantly increased, ~3-fold, in *Bhmt*-KO compared to WT liver (Fig. 4E and F; uncropped western blot Supplementary Fig. S1B).

2.5. *Bhmt-KO livers have increased FGF21 concentrations*

Since activated CREBH binds to the *Fgf21* promoter and results in its transcription [39], this could explain our earlier finding where *Bhmt*-KO mice, on a mixed 129/SV x C57BL/6J background (generations F3–F5), had increased FGF21 concentrations [7]. However, we now show that in fully backcrossed *Bhmt*-KO mice, compared to WT, plasma and hepatic FGF21 concentrations were increased more than 2-fold (Fig. 5A and B).

3. Discussion

The deletion of *Bhmt* in mice results in less fat storage in adipose tissue even though, to our knowledge BHMT is not expressed in adipose tissue, [7]. This adipose atrophy is the result of reduced triglyceride storage within iWAT associated with increased energy expenditure and heat production as measured by indirect calorimetry without a matching increase in food consumption [7]. We now report that elevated Hcy concentrations in *Bhmt*-KO correlate with the increase of ER stress signaling; resulting in the generation of activated CREBH, and increased expression of hepatic FGF21. Presumably, FGF21 is transported via circulation to adipocytes where it promotes the browning of white adipose tissue, increases expression of PGC-1α thus increasing mitochondrial number and expression of UCP-1, which uncouples mitochondrial respiration from ATP synthesis, thereby increasing energy expenditure and heat production (Fig. 6).

As noted earlier, BHMT catalyzes the formation of methionine from Hcy using betaine as a methyl donor [1,2]. Deletion of *Bhmt* increases concentrations of both substrates (betaine and Hcy) used by this enzyme. Increased concentrations of Hcy cause ER stress both *in vitro* and *in vivo* [26,27,29,32,33,36,40–42] by disrupting disulfide bond formation and thus leading to protein misfolding [27]. However, it is also possible that the accumulation of the other precursor, betaine, also contributes to adipocyte browning as feeding mice a diet containing 5% betaine increases plasma concentrations of FGF21 [7,43].

Since *Bhmt* deletion results in a reduced methylation potential by increasing *S*-adenosylhomocysteine concentrations, we had previously hypothesized that the FGF21 promoter region was could be hypomethylated in the *Bhmt*-KO mouse thereby explaining the increased expression ofFGF21. However, reduced representation bisulfite sequencing performed on liver DNA from WT and KO mice did not reveal any methylation differences in *FGF21* promoter [3].

ER stress is initiated by numerous metabolic stressors including high concentrations of homocysteine [26,27,29,32] and has been associated with hepatic lipid accumulation, obesity, cancer [30,44], and WAT browning [45]. Transcription factors that are regulated by ER stress include Sterol Regulatory Element Binding Proteins (SREBP) and CREBH [35], among others. CREBH can bind and activate FGF21 promoter at position −60 to −40 bp and has been shown to control the expression and plasma levels of FGF21 [39,46]. Additionally, FGF21 mediates many of CREBH's effects on fatty acid metabolism and ketogenesis [47]. Consistent with this, we did

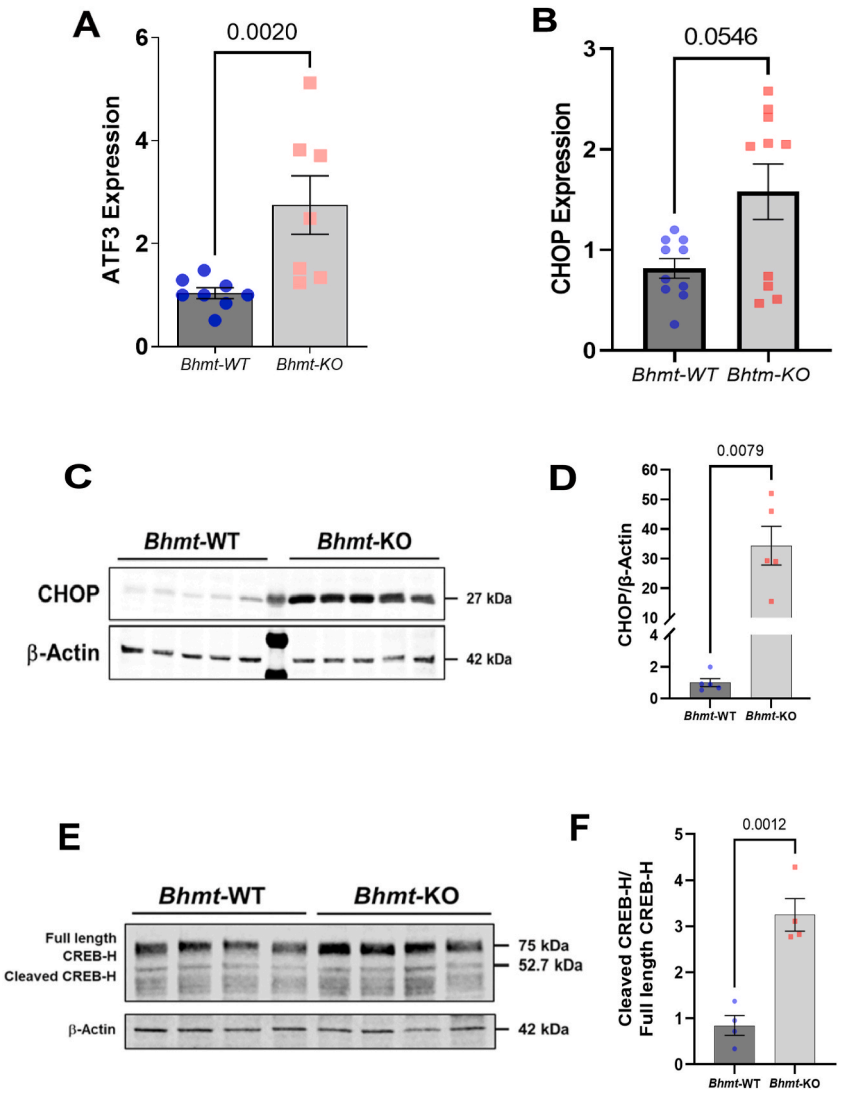

Fig. 4. Endoplasmic reticulum (ER) stress is increased in *Bhmt*-KO livers and exhibit activation of CREBH. (A) mRNA levels of ER stress markers *Atf3* are increased in liver *Bhmt*-KO mice compared to *Bhmt*-WT. $n = 7$ *Bhmt*-KO*;* $n = 8$ *Bhmt*-WT. P values were calculated by Mann-Whitney test. (B). Chop mRNA showed a tendency to be increased. P values were calculated by Kolmogorov-Smirnov. Relative quantitative values (normalized to 36B4) are reported as fold change. Results are presented as mean ± SEM. (C, D) Liver samples were examined by Western blot, were increased Chop protein levels were observed in *Bhmt*-KO vs *Bhmt*-WT. Actin was used as a loading control. Data are presented ad mean ± SEM. P values were calculated by Mann-Whitney test. n = 5 mice per group; per genotype. (E) Liver samples were examined by Western blot, to assess full-length CREBH and cleaved CREBH from *Bhmt*-WT and *Bhmt*-KO. Actin was used as a loading control. (F) The ratio of cleaved CREBH to full-length CREBH. n = 4 mice per group; per genotype. P values were calculated by unpaired *t*-test.

observe an increase in activated CREBH in *Bhmt*-KO mice. This study did not further investigate this association via deletion of CREBH, and cannot rule out the involvement of other pathways by which ER stress could alter FGF21 expression. Interestingly, in a *Fgf21-null* mouse model fed a methionine-choline deficient diet for one week, ER stress was enhanced identified by increased CHOP mRNA levels in liver. These results show the important role of FGF21 as a hepatoprotectant [48].

Many endocrine and autocrine signals stimulate adipose browning, including FGF21 [49]. FGF21 binds to its receptor (FGFR) and coreceptor β-Klotho (KLB) to activate a downstream signaling cascade that leads to the expression of its target genes [50]. FGF21 stimulates adipose browning and energy expenditure by upregulating the expression of transcriptional co-activator PGC-1α in adipose tissue [23,50,51]. Browning of white adipose tissue is characterized by the appearance of brown-like or beige adipocytes within WAT [52,53]. These inducible beige adipocytes are morphologically similar to brown adipocytes due to their expression of uncoupling protein 1 and contribution to thermogenesis [45,53].

In humans, serum FGF21 levels are associated with alcohol consumption, smoking [54] and prolonged fasting [55]. Other factors linked to the increase of serum FGF21 levels, in mice, are non-alcoholic steatohepatitis, improved glucose tolerance, and adverse lipid

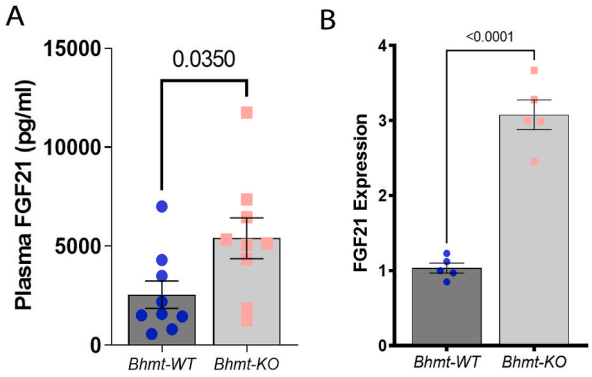

Fig. 5. FGF21 is increased in *Bhmt*-KO plasma and liver. (A) FGF21 levels are increased in plasma from *Bhmt*-KO mice when compared to *Bhmt*-WT. $n = 8$ per group. Results are represented as mean ± SEM. P values were calculated by *t*-test. (B) mRNA levels of Fgf21 in the liver are increased ~2 fold. Relative quantitative values (normalized to 36B4) are reported as fold change. P values were calculated by *t*-test. $N = 5$ per group.

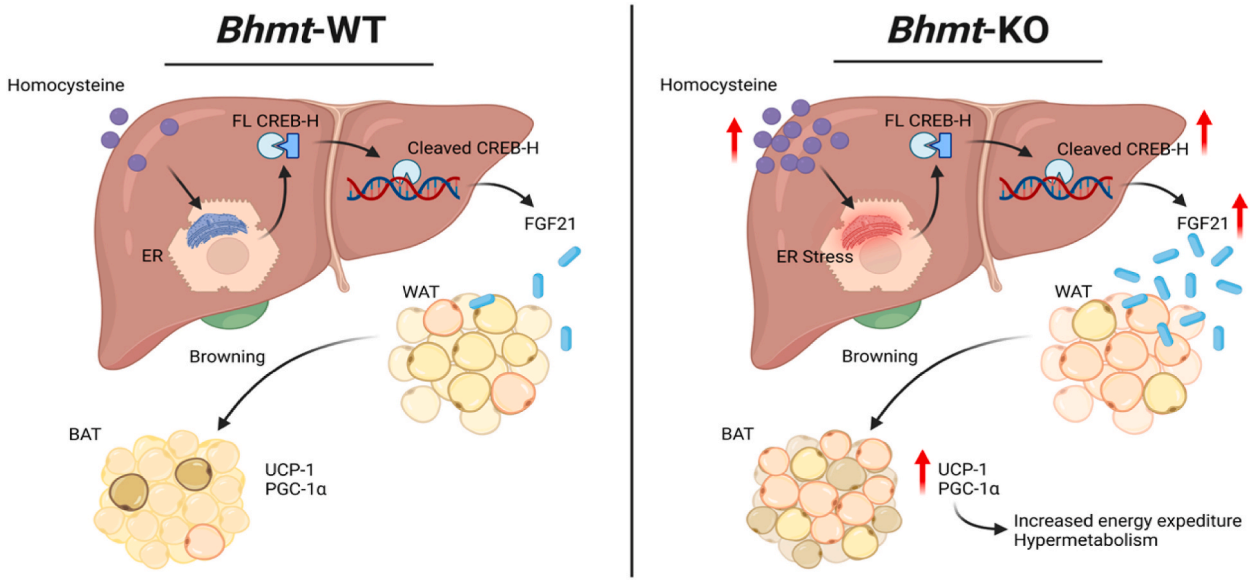

Fig. 6. Schematic representation of the effects of the deletion of *Bhmt* in liver and iWAT compared to *Bhmt*-WT. The schema summarizes our new findings where deletion of *Bhmt* in mice increases homocysteine levels leading to endoplasmic reticulum (ER) stress. ER stress led to an increase in the cleaved CREBH protein levels, which acts as a transcription factor that binds the FGF21 promoter. FGF21 high levels exert their effects in iWAT.

profiles [56,57]. Deletion of FGF21 in the liver drastically reduces circulating FGF21. At the same time, overexpression of FGF21 in adipocytes does not increase its circulating levels [58]. This suggests that the levels of serum FGF21 in the *Bhmt*-KO are a direct consequence of liver metabolism. It would be interesting to explore changes in FGF21 serum levels overtime in the *Bhmt*-KO model and study its association with other physiological responses. As noted, adipose atrophy is characterized by reduced fat/lean mass and the excessive 'slimming of adipocytes' in both size and volume [16]. Increased metabolic rate and adipose browning has been proposed as causes for adipose atrophy [8,16,18–20,59–63]. Even though browning of WAT is considered beneficial in obesity (reducing body weight and increasing energy expenditure), some evidence suggests that it also is associated with adverse outcomes such as hepatic steatosis, CAC, and burn-related cachexia [8,18,60,61].

The present study shows a novel phenotype of *Bhmt-KO* in adipose tissue. However, further research is needed to understand the phenotype. One of the limitations of our study is the lack of a CREBH knockout model to explore if we recapitulate, at least in part, the adipocyte phenotype we observed in the *Bhmt*-WT mice. Future studies are required to explore the potential liver-adipose tissue communication, lipolysis, and brown adipose tissue activation.

Is reduced BHMT expression likely to be a risk factor for people? Several functional *BHMT* variants have been identified in humans and are associated with increased risk for cancer and other diseases [64–67], however, no information is available on the metabolic phenotypes of humans carrying those variants. In mice, betaine supplementation delays muscle loss in an aging model [68], and more studies are needed to investigate if this happens in humans. In a meta-analysis of randomized controlled trials, betaine

supplementation is associated with reduced body fat mass and body fat percentage; however, no changes on BMI were reported [69]. It would be interesting to explore whether people with functional *BHMT* variants have a metabolic phenotype similar to that which we describe in mice. This would help us to understand how genetic variants in one carbon metabolism affect obesity and our understanding of how adipose atrophy develops in diseases such as cancer.

4. Materials and methods

4.1. Animals

Mice used in these experiments were bred and maintained at the David H. Murdock Research Institute (DHMRI), Center for Laboratory Animal Science facilities. All animal experiments were performed in accordance with the protocols approved by David H. Murdock Research Institute, Institutional Animal Care and Use Committee (IACUC).

Bhmt-KO mice were generated as previously described [5]. *Bhmt*-KO mice were fully backcrossed to C57B1/6 wild-type mice to generate a near congenic (99.73%) mouse line. For these studies our breeding pairs were (*Bhmt-WT; Bhmt-WT*) and (*Bhmt-KO; Bhmt-KO*). Genotyping of *Bhmt* animals was confirmed using the following primers: *Bhmt*-WT_F 5′–GACTTT TAAAGAGTGGTGGTACATACCTTG-3′, *Bhmt*-WT_R-5′ –TCTCTCTGCAGCCACATCTGAACTTGTCTG-3′, *Bhmt*-KO_F-5′ –TTAACTCAACATCACAACAACAGATTTCAG-3′, *Bhmt*-KO_R 5′ –TTG TCGACGGATCCATAACTTCGTATAAT-3′. *Bhmt*-WT and KO mice were mated and maintained *ad libitum* on an AIN 76A diet (Dyets, Bethlehem, PA, USA) and were kept in a temperature-controlled environment at 24 °C and exposed to a 12 h light and dark cycle. At 7–8 weeks, mice were fasted for 6 h and then euthanized by exposure to isoflurane. Tissue collection was performed for males and females, from both *Bhmt*-WT and *Bhmt*-KO, researchers were aware of the *Bhmt* genotype while performing experiments, except for the adipose tissue quantification (see details below).

4.2. Histological analysis

Tissues were fixed in buffered formalin, dehydrated in ethanol and then transferred to xylene solution for embedding in paraffin. Serial sections at 5 mm thickness were made from paraffin-embedded tissue and then stained with hematoxylin and eosin. Images were analyzed with light microscopy. Adipocyte area was calculated by measuring the area of cells per condition, using Image J (NIH, Bethesda, MD, USA). Researchers were blinded to mouse genotype and at least 50 cells were quantified per mouse, per genotype ($n = 3$ per group). Results are presented as mean ± SEM.

4.3. RT-PCR analysis

Total RNA was extracted from tissues of *Bhmt*-WT and *Bhmt*-KO mice, using RNAeasy mini-Kit (Qiagen, Hilden, Germany). cDNA synthesis was performed by using a Script™ cDNA SuperMix (Quanta BioSciences, Gaithrsburg, MD, USA). For quantitative real-time assays, amplification was performed by using PerfeCTa qPCR FastMix (Quanta Biosciences). We designed primers (Sigma) as follows: ***Ucp1*** forward primer: ACTGCCACAACCTCCAGTCATT, reverse primer CTTTGCCTCACTCAGGATTGG; **Pgc1a** forward primer AGCCGTGACCACTGACAACGAG, reverse primer GCTGCATGGTTCTGAGTGCTAGG; ***Cidea*** forward primer: GCAACCAAA-GAAATGCGGAATAG, reverse primer: CTCGTACATCGTGGCTTTGA; ***Chop*** forward primer CAGCGACAGAGCCAGAAT; ***Atf3*** forward primer GAGGCGGCGAGAAAGAAA, reverse primer CACACTCTCCAGTTTCTC. Ct values were calculated by SDS 1.2 software (Applied Biosystems, Foster City, CA, USA) and normalized to *36B4* Ct values and expressed as $2^{-(\text{Ct(gene)- Ct (housekeeping gene)})}$.

4.4. Western blot

Liver tissues were collected from *Bhmt*-WT and *Bhmt*-KO to evaluate CREBH and CHOP levels. Protein extracts were prepared using RIPA lysis buffer (Sigma, ST. Louis, USA) supplemented with protease inhibitor cocktail (Complete, Roche) and sonicated 50 oscillation/sec for 5 min (Tissue Lyser LT, Qiagen). Total protein concentrations for all samples were quantified using BSA standards (catalog number A7030, Sigma-Aldrich). Proteins were loaded into SDS-PAGE gels and blotted on nitrocellulose. Membranes were immersed in blocking solution (BSA 5%; catalog number 03116956001, Sigma; TBS 1x and 0.1% Tween-20) for 1 h. CREBH antibody (catalog number: EWS10. Kerafast; Boston, MA, USA.) was used at 1:1000 dilution, overnight incubation. CHOP (catalog number 5554. Cell Signaling Technology, US.) was used 1:1000, overnight incubation. Beta actin (catalog number ab8226. Abcam, Boston, MA, USA.) was used 1:1000 for 1 h incubation at room temperature. The secondary antibodies were IRDye 800CW goat anti-rabbit IgG (catalog number 926-322. Li-Cor Biosciences, Lincoln, NE, US) and goat anti-mouse IgG IRDye 680RD (926-68070. Li-Cor Biosciences). The membranes were imaged in a Li-Cor Odyssey imaging system and protein abundance was quantified using the Image Studio Lite (Li-Cor Biosciences, version 5.2.5, 2015). Data are presented by mean ± SEM.

4.5. FGF21 and Homocysteine measurement

4.5.1. Serum

Blood samples from *Bhmt*-WT and *Bhmt*-KO mice, were collected and centrifuged at 1000 g for 15 min at 4 °C. **Liver**: Crushed liver samples were homogenized in cold phosphate-buffered saline (PBS, Sigma) with protease inhibitors (Roche). Samples were centrifuged at 9600 g for 15 min at 4 °C. For both plasma and liver, supernatant protein was quantified using BCA protein assay (Bio-Rad, Hercules,

CA, USA) and diluted to equal concentrations before performing an enzyme-linked immunosorbent assay (ELISA) using a Mouse/Rat FGF21 Quantikine ELISA kit (R&D Systems, Minneapolis, MN) [70].

4.5.2. Homocysteine measurement

Plasma or liver, from *Bhmt*-WT and *Bhmt*-KO was homogenized in dithiothreitol (DTT) and processed to dissociate the proteins by filtration, thereby extracting protein-bound Hcy. The protein-free filtrate was analyzed for total Hcy by liquid chromatography-electrospray ionization-tandem mass spectrometry (LC-ESI-MS/MS) as previously described [71,72].

4.5.3. Statistical analysis

The number of samples per group are indicated in the figure legends. There were no experimental units or data points excluded. Statistical analyses were performed with Prism 7 (GraphPad Software, La Jolla, CA, USA). Data distribution was tested for statistical normality. The Brown-Forsythe test (F test) was used to compare group variances. Groups with equal distribution were compared using Students' *t*-test. Groups with unequal variances were compared using no-*n*-parametric tests and it is indicated on the figure legend. Data are presented as means ± SEM and p values are reported on each graph.

Author contribution statement

Manya Warrier, Isis Trujillo-Gonzalez: Conceived and designed the experiments; Performed the experiments; Analyzed and interpreted the data; Wrote the paper.

Evan M. Paules, Jorge Silva-Gomez: Performed the experiments; Wrote the paper.

Walter B. Friday, Frances Bramlett, Hyunbae Kim: Performed the experiments.

Kezhong Zhang: Performed the experiments; Analyzed and interpreted the data.

Funding statement

This work was supported by National Institute of Diabetes and Digestive and Kidney Diseases [DK056350 & DK115380].

Data availability statement

Data included in article/supp. material/referenced in article.

Declaration of interest's statement

The authors declare the following conflict of interests: Jorge Silva-Gomez is a Balchem Postdoctoral Fellow. Balchem had no role in the study design, data collection, analysis or preparation of the manuscript. The rest of the authors report no conflicts of interest.

Acknowledgments

The authors thank Jennifer Owen (University of North Carolina at Chapel Hill, Nutrition Research Institute) for providing assistance with experiments; Dr. Steve Orena (University of North Carolina at Chapel Hill, Nutrition Research Institute) for providing metabolite services. Dr. Blanca Castro Magdonel (University of North Carolina at Chapel Hill, Nutrition Research Institute), assisted with blinded area quantification of adipocytes. The authors thank Dr. David Horita (Nutrition Research Institute) for critically evaluating the manuscript and Dr. Steve H. Zeisel (University of North Carolina at Chapel Hill, Nutrition Research Institute) for suggestions, mentoring, and critically evaluating the manuscript. This work was supported by the US National Institutes of Health (NIH), National Institute of Diabetes and Digestive and Kidney Diseases Grants DK056350 and DK115380 (To Dr. Steven H. Zeisel).

Appendix A. Supplementary data

Supplementary data to this article can be found online at https://doi.org/10.1016/j.heliyon.2023.e13216.

References

[1] M.F. Abdelmalek, et al., Betaine, a promising new agent for patients with nonalcoholic steatohepatitis: results of a pilot study, Am. J. Gastroenterol. 96 (9) (2001) 2711–2717.

[2] K. Zhang, et al., Endoplasmic reticulum stress activates cleavage of CREBH to induce a systemic inflammatory response role of endoplasmic reticulum stress and unfolded protein responses in Health and diseases, Cell 124 (3) (2006) 587–599.

[3] D.S. Lupu, et al., Altered methylation of specific DNA loci in the liver of Bhmt-null mice results in repression of Iqgap2 and F2rl2 and is associated with development of preneoplastic foci, Faseb. J. 31 (5) (2017) 2090–2103.

[4] M.A. Pajares, D. Perez-Sala, Betaine homocysteine S-methyltransferase: just a regulator of homocysteine metabolism? Cell. Mol. Life Sci. 63 (23) (2006) 2792–2803.

[5] Y.W. Teng, et al., Deletion of betaine-homocysteine S-methyltransferase in mice perturbs choline and 1-carbon metabolism, resulting in fatty liver and hepatocellular carcinomas, J. Biol. Chem. 286 (42) (2011) 36258–36267.
[6] R.S. Ganu, et al., Molecular characterization and analysis of the porcine betaine homocysteine methyltransferase and betaine homocysteine methyltransferase-2 genes, Gene 473 (2) (2011) 133–138.
[7] Y.W. Teng, et al., Mouse betaine-homocysteine S-methyltransferase deficiency reduces body fat via increasing energy expenditure and impairing lipid synthesis and enhancing glucose oxidation in white adipose tissue, J. Biol. Chem. 287 (20) (2012) 16187–16198.
[8] M. Petruzzelli, et al., A switch from white to brown fat increases energy expenditure in cancer-associated cachexia, Cell Metabol. 20 (3) (2014) 433–447.
[9] J. Nedergaard, B. Cannon, The browning of white adipose tissue: some burning issues, Cell Metabol. 20 (3) (2014) 396–407.
[10] F.M. Fisher, E. Maratos-Flier, Understanding the physiology of FGF21, Annu. Rev. Physiol. 78 (2016) 223–241.
[11] M. Defour, et al., The peroxisome proliferator-activated receptor α is dispensable for cold-induced adipose tissue browning in mice, Mol. Metabol. 10 (2018) 39–54.
[12] M.-K. Lee, B. Lee, C.Y. Kim, Natural extracts that stimulate adipocyte browning and their underlying mechanisms, Antioxidants 10 (2) (2021) 308.
[13] K.A. Lo, L. Sun, Turning WAT into BAT: a review on regulators controlling the browning of white adipocytes, Biosci. Rep. 33 (5) (2013).
[14] S. Kir, et al., Tumour-derived PTH-related protein triggers adipose tissue browning and cancer cachexia, Nature 513 (7516) (2014) 100–104.
[15] J. Stockli, et al., Metabolomic analysis of insulin resistance across different mouse strains and diets, J. Biol. Chem. 292 (47) (2017) 19135–19145.
[16] C. Bing, P. Trayhurn, New insights into adipose tissue atrophy in cancer cachexia, Proc. Nutr. Soc. 68 (4) (2009) 385–392.
[17] A. Peschechera, J. Eckel, Browning" of adipose tissue–regulation and therapeutic perspectives, Arch. Physiol. Biochem. 119 (4) (2013) 151–160.
[18] M. Petruzzelli, E.F. Wagner, Mechanisms of metabolic dysfunction in cancer-associated cachexia, Genes Dev. 30 (5) (2016) 489–501.
[19] J. Han, et al., Interleukin-6 induces fat loss in cancer cachexia by promoting white adipose tissue lipolysis and browning, Lipids Health Dis. 17 (1) (2018) 14.
[20] S. Kir, et al., PTH/PTHrP receptor mediates cachexia in models of kidney failure and cancer, Cell Metabol. 23 (2) (2016) 315–323.
[21] H. Ohno, et al., EHMT1 controls brown adipose cell fate and thermogenesis through the PRDM16 complex, Nature 504 (7478) (2013) 163–167.
[22] M. Defour, et al., The Peroxisome Proliferator-Activated Receptor alpha is dispensable for cold-induced adipose tissue browning in mice, Mol. Metabol. 10 (2018) 39–54.
[23] F.M. Fisher, et al., FGF21 regulates PGC-1alpha and browning of white adipose tissues in adaptive thermogenesis, Genes Dev. 26 (3) (2012) 271–281.
[24] S.M. Colgan, A.A. Hashimi, R.C. Austin, Endoplasmic reticulum stress and lipid dysregulation, Expet Rev. Mol. Med. 13 (2011) e4.
[25] M. Wang, S. Zhao, M. Tan, bZIP transmembrane transcription factor CREBH: potential role in non-alcoholic fatty liver disease (Review), Mol. Med. Rep. 13 (2) (2016) 1455–1462.
[26] Y. Ai, et al., Homocysteine induces hepatic steatosis involving ER stress response in high methionine diet-fed mice, Nutrients 9 (4) (2017).
[27] N. Dionisio, et al., Homocysteine, intracellular signaling and thrombotic disorders, Curr. Med. Chem. 17 (27) (2010) 3109–3119.
[28] P.L. Faust, W.J. Kovacs, Cholesterol biosynthesis and ER stress in peroxisome deficiency, Biochimie 98 (2014) 75–85.
[29] N. Kaplowitz, et al., Endoplasmic reticulum stress and liver injury, Semin. Liver Dis. 27 (4) (2007) 367–377.
[30] C. Lebeaupin, et al., Endoplasmic reticulum stress signaling and the pathogenesis of non-alcoholic fatty liver disease, J. Hepatol. 69 (4) (2018) 927–947.
[31] A.A. Mahdi, S.H. Rizvi, A. Parveen, Role of endoplasmic reticulum stress and unfolded protein responses in Health and diseases, Indian J. Clin. Biochem. 31 (2) (2016) 127–137.
[32] C.Y. Wang, et al., Hydrogen sulfide prevents homocysteine induced endoplasmic reticulum stress in PC12 cells by upregulating SIRT1, Mol. Med. Rep. 16 (3) (2017) 3587–3593.
[33] G.H. Werstuck, et al., Homocysteine-induced endoplasmic reticulum stress causes dysregulation of the cholesterol and triglyceride biosynthetic pathways, J. Clin. Invest. 107 (10) (2001) 1263–1273.
[34] C. Zhang, et al., Endoplasmic reticulum stress is involved in hepatic SREBP-1c activation and lipid accumulation in fructose-fed mice, Toxicol. Lett. 212 (3) (2012) 229–240.
[35] K. Zhang, et al., Endoplasmic reticulum stress activates cleavage of CREBH to induce a systemic inflammatory response, Cell 124 (3) (2006) 587–599.
[36] Z. Zhang, et al., Homocysteine induces apoptosis of human umbilical vein endothelial cells via mitochondrial dysfunction and endoplasmic reticulum stress, Oxid. Med. Cell. Longev. 2017 (2017), 5736506.
[37] Y. Nakagawa, et al., Hepatic CREB3L3 controls whole-body energy homeostasis and improves obesity and diabetes, Endocrinology 155 (12) (2014) 4706–4719.
[38] J.G. Park, et al., CREBH-FGF21 axis improves hepatic steatosis by suppressing adipose tissue lipolysis, Sci. Rep. 6 (2016), 27938.
[39] H. Kim, et al., Liver-enriched transcription factor CREBH interacts with peroxisome proliferator-activated receptor alpha to regulate metabolic hormone FGF21, Endocrinology 155 (3) (2014) 769–782.
[40] P.A. Outinen, et al., Characterization of the stress-inducing effects of homocysteine, Biochem. J. 332 (Pt 1) (1998) 213–221.
[41] P.A. Outinen, et al., Homocysteine-induced endoplasmic reticulum stress and growth arrest leads to specific changes in gene expression in human vascular endothelial cells, Blood 94 (3) (1999) 959–967.
[42] M. Curro, et al., Homocysteine-induced toxicity increases TG2 expression in Neuro2a cells, Amino Acids 36 (4) (2009) 725–730.
[43] A. Ejaz, et al., Dietary betaine supplementation increases Fgf21 levels to improve glucose homeostasis and reduce hepatic lipid accumulation in mice, Diabetes 65 (4) (2016) 902–912.
[44] S.A. Oakes, F.R. Papa, The role of endoplasmic reticulum stress in human pathology, Annu. Rev. Pathol. 10 (2015) 173–194.
[45] A. Abdullahi, M.G. Jeschke, White adipose tissue browning: a double-edged sword, Trends Endocrinol. Metabol. 27 (8) (2016) 542–552.
[46] Y. Nakagawa, et al., Hepatic CREB3L3 controls whole-body energy homeostasis and improves obesity and diabetes CREB3L3 controls fatty acid oxidation and ketogenesis in synergy with PPARalpha, Endocrinology 155 (12) (2014) 4706–4719.
[47] Y. Nakagawa, et al., CREB3L3 controls fatty acid oxidation and ketogenesis in synergy with PPARalpha, Sci. Rep. 6 (2016), 39182.
[48] N. Tanaka, et al., Role of fibroblast growth factor 21 in the early stage of NASH induced by methionine- and choline-deficient diet, Biochim. Biophys. Acta (BBA) - Mol. Basis Dis. 1852 (7) (2015) 1242–1252.
[49] J. Hu, M. Christian, Hormonal factors in the control of the browning of white adipose tissue, Horm. Mol. Biol. Clin. Invest. 31 (1) (2017).
[50] N. Itoh, FGF21 as a hepatokine, adipokine, and myokine in metabolism and diseases, Front. Endocrinol.(Lausanne) 5 (2014) 107.
[51] M.J. Potthoff, et al., FGF21 induces PGC-1alpha and regulates carbohydrate and fatty acid metabolism during the adaptive starvation response, Proc. Natl. Acad. Sci. U. S. A. 106 (26) (2009) 10853–10858.
[52] D.M. Sepa-Kishi, R.B. Ceddia, White and beige adipocytes: are they metabolically distinct? Horm. Mol. Biol. Clin. Invest. 33 (2) (2018).
[53] D.M. Sepa-Kishi, et al., White and beige adipocytes: are they metabolically distinct? Physiological regulation and metabolic role of browning in white adipose tissue, Horm. Mol. Biol. Clin. Invest. 33 (2) (2018).
[54] K. Nakanishi, et al., Serum FGF21 levels are altered by various factors including lifestyle behaviors in male subjects, Sci. Rep. 11 (1) (2021), 22632.
[55] C. Gälman, et al., The circulating metabolic regulator FGF21 is induced by prolonged fasting and PPARα activation in man, Cell Metabol. 8 (2) (2008) 169–174.
[56] S. Epperlein, et al., The effect of FGF21 and its genetic variants on food and drug cravings, adipokines and metabolic traits, Biomedicines 9 (4) (2021) 345.
[57] Y. Lee, et al., Serum FGF 21 concentration is associated with hypertriglyceridaemia, hyperinsulinaemia and pericardial fat accumulation, independently of obesity, but not with current coronary artery status, Clin. Endocrinol. 80 (1) (2014) 57–64.
[58] M. Abu-Odeh, et al., FGF21 promotes thermogenic gene expression as an autocrine factor in adipocytes, Cell Rep. 35 (13) (2021), 109331.
[59] J.A. Vaitkus, F.S. Celi, The role of adipose tissue in cancer-associated cachexia, Exp. Biol. Med. (Maywood) 242 (5) (2017) 473–481.
[60] J.M. Argiles, et al., Cancer cachexia: understanding the molecular basis, Nat. Rev. Cancer 14 (11) (2014) 754–762.
[61] S. Kir, B.M. Spiegelman, Cachexia & brown fat: a burning issue in cancer, Trends Cancer 2 (9) (2016) 461–463.
[62] A. Kulyte, et al., MicroRNA profiling links miR-378 to enhanced adipocyte lipolysis in human cancer cachexia, Am. J. Physiol. Endocrinol. Metab. 306 (3) (2014) E267–E274.
[63] A. Vegiopoulos, M. Rohm, S. Herzig, Adipose tissue: between the extremes, EMBO J. 36 (14) (2017) 1999–2017.

[64] H. Pellanda, et al., A splicing variant leads to complete loss of function of betaine-homocysteine methyltransferase (BHMT) gene in hepatocellular carcinoma, Int. J. Biochem. Cell Biol. 44 (2) (2012) 385–392.
[65] T.M. Gibson, et al., Comprehensive evaluation of one-carbon metabolism pathway gene variants and renal cell cancer risk, PLoS One 6 (10) (2011), e26165.
[66] Q. Feng, et al., Betaine-homocysteine methyltransferase: human liver genotype-phenotype correlation, Mol. Genet. Metabol. 102 (2) (2011) 126–133.
[67] F. Li, et al., Human betaine-homocysteine methyltransferase (BHMT) and BHMT2: common gene sequence variation and functional characterization, Mol. Genet. Metabol. 94 (3) (2008) 326–335.
[68] S. Chen, et al., Betaine delayed muscle loss by attenuating samtor complex inhibition for mTORC1 signaling via increasing SAM level, Mol. Nutr. Food Res. 65 (15) (2021) e2100157.
[69] X. Gao, et al., Effect of betaine on reducing body fat—a systematic review and meta-analysis of randomized controlled trials, Nutrients 11 (10) (2019) 2480.
[70] A. Archer, et al., Fasting-induced FGF21 is repressed by LXR activation via recruitment of an HDAC3 corepressor complex in mice, Mol. Endocrinol. 26 (12) (2012) 1980–1990.
[71] S.-C. Lai, et al., The transcobalamin receptor knockout mouse: a model for vitamin B12 deficiency in the central nervous system, Faseb. J. 27 (6) (2013) 2468–2475.
[72] V. Ducros, et al., A robust liquid chromatography tandem mass spectrometry method for total plasma homocysteine determination in clinical practice, Clin. Chem. Lab. Med. 44 (8) (2006) 987–990.